PhiDsc: Protein functional mutation Identification by 3D Structure Comparison

Mohamad Hussein Hoballa [1] and Changiz Eslahchi[1*]

1 Department of Computer Science, Shahid Beheshti University, Evin, Tehran, 1983963113 Iran

* To whom correspondence should be addressed. Tel: +98 21 22431653; Email: ch-eslahchi@sbu.ac.ir

Selective pressures that trigger cancer formation and progression shape the mutational landscape of somatic mutations in cancer. Given the limits within which cells are regulated, a growing tumor has access to only a finite number of pathways that it can alter. As a result, tumors arising from different cells of origin often harbor identical genetic alterations. Recent expansive sequencing efforts have identified recurrent hotspot mutated residues in individual genes. Here, we introduce PhiDsc, a novel statistical method developed based on the hypothesis that, functional mutations in a recurrently aberrant gene family can guide the identification of mutated residues in the family's individual genes, with potential functional relevance. PhiDsc combines 3D structural alignment of related proteins with recurrence data for their mutated residues, to calculate the probability of randomness of the proposed mutation. The application of this approach to the RAS and RHO protein families returned known mutational hotspots as well as previously unrecognized mutated residues with potentially altering effect on protein stability and function. These mutations were located in, or in proximity to, active domains and were indicated as protein-altering according to six *in silico* predictors. PhiDsc is freely available at https://github.com/hobzy987/PhiDSC-DALI.

INTRODUCTION

Cancer development starts with the acquisition of genomic alterations and chromosomal abnormalities that arise from uncorrected errors during DNA replication or repair or due to exposure to mutagens (1). Some alterations may further the accumulation of somatic mutations (2) and play a mechanistic role in malignant transformation. These "driver mutations" are postulated to provide advantage to and promote cancer hallmarks in the subpopulation of cells that harbor them (3). The number of driver mutations varies between cancer types, averaging four per tumor (4). Most remaining somatic alterations, termed "passenger mutations," may confer little to no functional impact (5). However, distinguishing the handful of driver mutations from the vast background of passenger mutations in a tumor has remained a challenge in cancer genomics.

Frequently altered nucleotides in the genes that are implicated in tumor development and progression are known as mutational hotspots (6). The number of candidate hotspot mutations of unknown functional significance has increased recently –especially due to the completion of large-scale sequencing efforts such as The Cancer Genome Atlas (TCGA) (7), International Cancer Genome Consortium (ICGC) (8), and Project GENIE (9). Many platforms are used to visualize and organize these data like BioMuta (10) and cBioPortal(11, 12) allowing to download and analyze large-scale cancer genomics datasets. Most of these frequently detected mutations are within exons, or the coding regions of the proteins, and their function is ascertained by directly examining their impact on the encoded protein or predicted through application of *in silico* bioinformatic approaches (13, 14).

The statistical reoccurrence of mutations in tumors has been used as an indicator of their functional impact, based on the assumption that infrequent alterations detected in tumors are likely non-functional, passenger events (15). However, it has been shown that passenger mutations are not

randomly distributed along the cancer genomes (16). Rather, they are enriched in nucleotide sequence contexts that are shaped by specific active mutational processes in a tumor (17, 18). In contrast, driver mutations are postulated to occur in genomic positions whose distribution depends not only on the local nucleotide context, but also on the location of functionally relevant residues along the protein sequence (19, 20). Relying on recurrence alone to identify functional mutations, may also be confounded by underlying mutational processes that target specific genomic contexts, resulting in often-mutated residues that do not drive tumor progression (21).

In this context, numerous methods are presently being used to identify hotspot and driver mutations, based on the frequency of mutations detected in a gene across a set of tumor samples (e.g., MutSig (22) and MuSiC (23)). Recognizing mutational hotspot in infrequently altered genes can also be refined by including protein-level annotation by local-positional clustering (24), or the inclusion of phosphorylation sites (25) and information from paralogous protein domains (26). Protein-level annotation, such as local-positional clustering, phosphorylation sites, and paralogous protein domain (27) as well as 3D protein structures are used to identify functional mutations in infrequently mutated genes.

Using a variety of approaches that take into account diverse aspects of protein structures and types, functional mutations can be predicted across protein sequences and structures. Some techniques, such as 3DHotspots (28), Hotspot3D (29), Mutation3D (30), and Signatures of Cancer Mutation Hotspots in Protein Kinases (31) use the 3D structure of protein, while others utilize 3D reconstruction of protein networks to provide a better understanding of genetic abnormalities (32). On the other hand, methods like PinSnps (33), StructMAn (34), Hot-MAPS (35) and SpacePAC (36), as well as SAAMBE-3D(37), use protein-protein interactions enriched with somatic cancer mutations (38) to understand the effect of a mutation not only on the

function of the same protein but also on the signal transduction and activating cascade proteins. Methods based on individual protein structures or the 3D reconstruction of protein networks have improved the identification of mutational clusters in tumors (39) and have elucidated functional consequences (folding free energy and stability of protein monomers (40)) of protein-altering mutations, other methods take into consideration the local DNA sequence context for the analysis of cancer context-dependent mutations like MutaGene(41). Although it is difficult to categorize methods based on their input parameters (some require sequences while others may need structures as well), in all cases, the output determines whether a proposed mutation has occurred at a hotspot residue. However, a few limitations remain: First, focusing on the mutation frequency across tumor samples increases the risk of missing portions of rare hotspot mutations with low frequency; second, concentrating solely on driver genes fails to distinguish between individual driver mutations within altered genes and passenger mutations within the same gene; and third, analyzing protein sequences without a larger context misses the effect of mutations on the conformational structure and functional sites of the protein.

To address these issues, we introduce PhiDsc. Its development is based on the hypothesis that oncogenic mutations in a target protein can be identified by analyzing its three-dimensional structural similarity, protein folding information, and mutational recurrence within its gene family. We demonstrate that PhiDsc can identify candidate functional mutations, caused on altered protein position, by comparing the three-dimensional structures of related human wild-type proteins and assessing repeatedly altered residues in the protein family. PhiDsc combines the two approaches by relying on the concept of hotspot mutations in functional regions and classifying protein families based on their domains and active sites. Thus, by comparing the three-dimensional structures of similar domains within a protein family, PhiDsc maps known functional mutations in extensively studied proteins to those in the family that receive less interest.

RESULTS

PhiDsc is applied to HRAS from the RAS (59) subfamily and RhoA from the RHO (60) subfamily of proteins.

HRAS

The family group of HRAS was A(HRAS) = {DIRAS1, DIRAS2, GEM, KRAS, NRAS, RAP1A, RAP1B, RAP2A, RASL12, REM1, REM2, RERG, RRAD, RRAS, RRAS2}. Dali aligned 98% of HRAS residues to residues of each member of the family **(Table 1)** highlighting strong structural similarity between the target protein and its respective protein families. (Supplementary files HRAS alignment). As a result, PhiDsc scored 168 of 189 HRAS residues (89%) and predicted 13 residues as functional mutation (**Table 2**) all of which passed cross-validation evaluation

(**Figure 1**) and were consistently projected to be effective and protein-modifying by six independent algorithms.

Table 1 indicates the percentage of structural alignment between each protein (HRAS) and its protein family member.

	HRAS											
Protein	RALA	RALB	RAP1A	RAP1B	RAP2A	KRAS	RASL12	NRAS	RERG	RIT1	RRAS2	RRAS	Median
PDB ID	2BOV	2KWI	1C1Y	4DXA	1KAO	3GFT	3C5C	3CON	2ATV	4KLZ	2ERY	2FN4	
Alignment	100	100	97.619	98.214	98.214	98.809	95.238	92.857	98.809	92.261	97.619	100	98.214

Table 2 Candidate functional mutations for HRAS proposed by PhiDsc. Residue positions sorted by their PhiDsc score p-value along with predicted interacting residues from the RIN analysis are shown. COSMIC mutation reference or dbSNP polymorphism ID are

also shown when available.

HRAS											
Residue Nu	P-value	Interacting Residue									mut ref Nu
12	2.66E-07	11	16								COSM483
74	1.72E-06	5	70	71	73	75					COSM5991570
13	2.57E-06	117									COSM486
93	6.18E-06	81	82	90	91	113	137				COSM9497546
91	8.72E-06	87	88	90	93	95					COSM6476473
22	1.38E-05	18	19	20	32	26	28	146	149	152	COSM6923245
96	1.54E-05	9	10	11	92	93	97	98	99	100	RS889495169
117	1.85E-05	13	14	83	84	116	119	120	144		CSOM304967
31	3.84E-05	30	33								COSM6915342
40	4.20E-05	20	24	32	38	39	54	55	57		RS763920334
155	5.08E-05	79	144	151	152	153	159				COSM9515051
148	5.23E-05	119	145	150							COSM6903495
38	5.93E-05	39	40	57							RS750680771

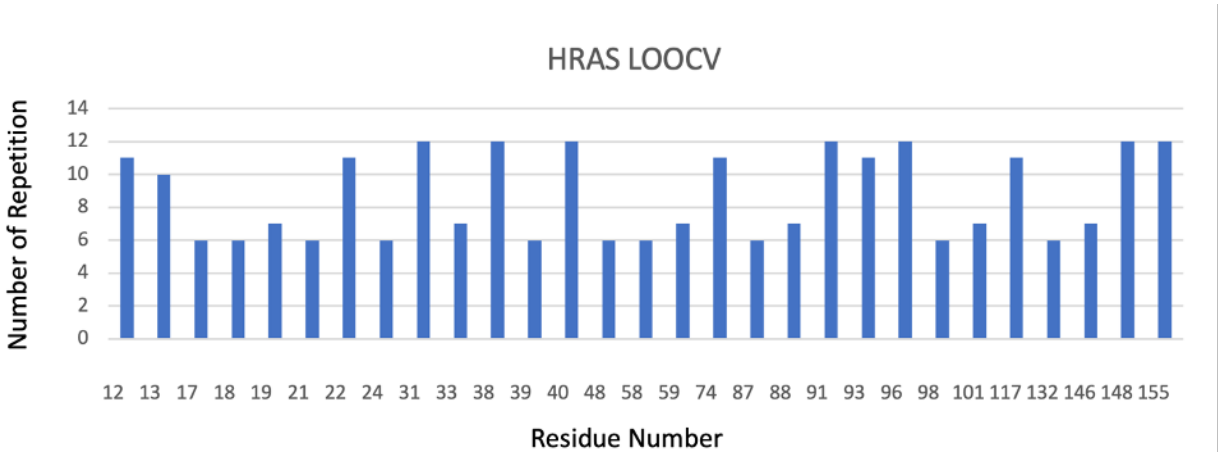

Figure 1 shows the LOOCV for the two proteins HRAS, in all the iterations of the system the number of repeated times for each residue is shown, (>80%), which indicates that the results obtained by the system are robust since the original results are obtained in all the LOOCV iteration

RIN is generated using the HRAS structure (RCSB database ID 4Q21, with 168 residues). Thirteen candidate functional mutations shared 58 neighboring residues located in the functional domains of the protein (G boxes, Switches I and II, GDI and GEF interaction sites, GTP/MG2+ binding domain). Moreover, 25 of these 58 residues were seen mutated in human tumors according to the cBioPortal(11, 12) database a distinct dataset form BioMuta.

Top-four PhiDsc predictions in HRAS were residues 12, 13, 74, and 93, which are known to be key functionals and often mutated in various cancer types (61). The domain comprising residues 12 and 13 is involved in Guanine Nucleotide Dissociation Inhibitor (GDI) interaction as well as interaction with GTP/Mg2+ (62), and is mostly detected in tumors such as bladder cancer (63), thyroid cancer(64), and other diseases such as Costello syndrome (61) and Schimmelpenning-Feuerstein-Mims syndrome (63, 65). Mutations in residue 74 are seen in endometrioid cancer and sebaceous carcinoma, while those in residue 93, have been discovered in only a small percentage of prostate cancer samples (66). According to Ensemble Learning Approach for Stability Prediction of Interface and Core mutations (ELSPIC) (67), residue 93 is localized in the protein's core, suggesting that it has a direct effect on the protein's shape and function.

Although 3 of 13 candidate functional mutations in HRAS were not located in any protein domains, they were found near the intersection of exons 3 and 4 at residue 97. Finally, residue 96 has been identified as a phosphorylation site, the other residues as showen in (**Figure 2**) were located in functional protein domains.

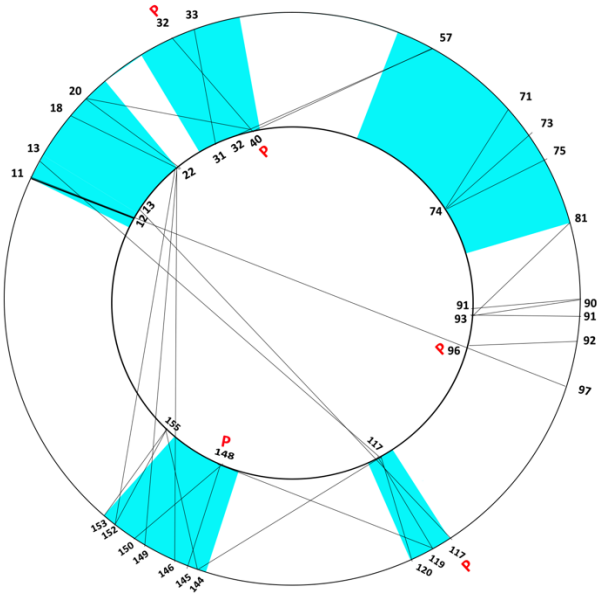

Figure 2 depicts the inner circle's candidate functional mutations and the outer circle's interacting residues. According to thecanSAR BLACK system (60), The blue areas represent HRAS functional regions, while the lines linking the inner circle (candidate functio functional mutation) to the outer circle (interacting residues) represent residue interactions. This figure displays only the HRAS residues that are mutated in cBioPortal.

RhoA

RhoA, a member of the RHO (60) subfamily of proteins with A(RhoA) = {RHOB, RHOC, RHOD, RHOQ, RHOU, RND1, RND3, RAC1, RAC2, RAC3, CDC42}.

The RCSB database is used to retrieve 3D structure files for each member (if found in PDB) of A(RhoA). The final list of PDB structures are shown in **Table 3**. The Dali server is then used to perform a pairwise structural comparison between the input protein and each member of its family. 97% of RhoA residues were aligned with the residues of each family member in the generated alignments. The existence of strong structural similarities between target proteins and their respective protein families supports these results (Supplementary file “RhoA alignment”).

As an outcome, 179 out of 193 residues were scored for RhoA.

Table 3 shows the percentage of structural alignment of each protein (RhoA) with its corresponding protein family member.

	RHOA										
Protein	RAC1	RAC2	RAC3	RHOB	RHOC	RHOD	RHOQ	RHOU	RND1	RND3	Median
PDB ID	1E96	1DS6	2C2H	2FV8	2GCN	2J1L	2ATX	2Q3H	3Q3J	2V55	
Alignment	99.441	99.441	93.854	95.53	98.324	87.709	99.441	94.413	97.206	100	97.765

The P-value of PhiDsc statistics is generated for all target protein residues in the final phase. Eight candidate functional mutations for RhoA were obtained. **Table 4** illustrates the RhoA protein candidate functional mutations introduced by the PhiDsc procedure. The eight candidates passed cross validation (**see Figure 3**) and were consistently predicted to be effective and protein-modifying by six separate algorithms. Despite the fact that no evidence of a mutation in residue 29 of RhoA was detected in any cancer mutation databases, all six techniques predicted that this mutation would alter RhoA's functional activity.

Table 4 lists all candidate functional mutations for RhoA proposed by the PhiDsc approach. The table shows the residue position number (P) in the first column, sorted by their P-value in the second column, the interacting residues of each candidate functional mutation in the third column, the "COSM" letters of the mutations indicate that these mutations were annotated in the cosmic database as tumor-related mutations, while the "rs" letters of the mutations indicate that these mutations were annotated in the Dpsnp database.

RHOA										
Residue Number	P-value	interacting residue								mutation ref NU
111	3.07904E-05	78	79	80	109	110	177			COSM2849881
34	4.86819E-05	35								COSM2849895
139	9.956E-05	84	86	89	92	122	139	140	143	COSM2849897
168	0.000147858	170	171	172						COSM7114068
110	0.000209526	77	78	79	80	107	108	11		RS368767616
29	0.000224094	23	27	28	29	31				NO
172	0.000300752	46	48	168	169	172	174	175	176	COSM1309264
127	0.000484266	87	121	124	125	127	129	130	131	MU85445108

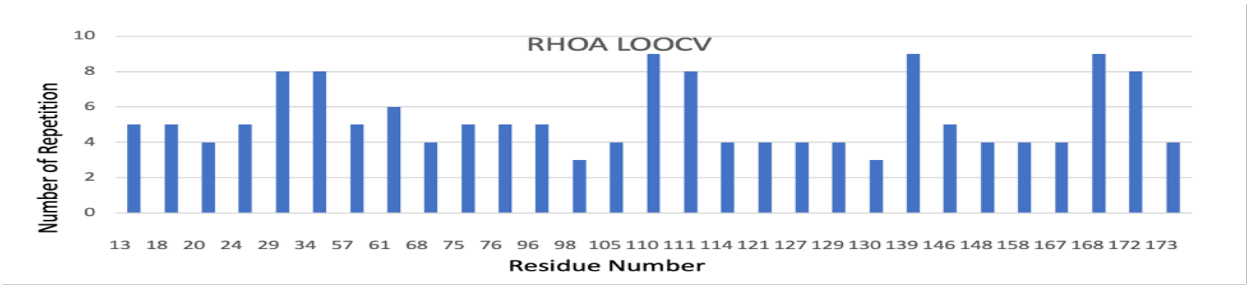

Figure 3 shows the LOOCV for the protein RhoA; the number of repeated times for each residue is presented in all iterations of the system, indicating that the system's results are resilient because the original results are obtained in all LOOCV iterations.

The RIN for RhoA is constructed using 1OW3 obtained from the RCSB database. The 8 potential functional mutations have 42 neighbors, 18 of which had previously been identified as occurring mutations in the cBioPortal database (11, 12) (**see Table 3/interacting residues**). The neighbors of potential functional mutations are related to PPI functionals, according to RINalyzer data. These neighbors are also located in RhoA protein domains associated to GAP, GEF, and GDI interaction and phosphorylation sites, including position 127—showing that this residue is significant in RhoA's functional activity (**see Figure 4**).

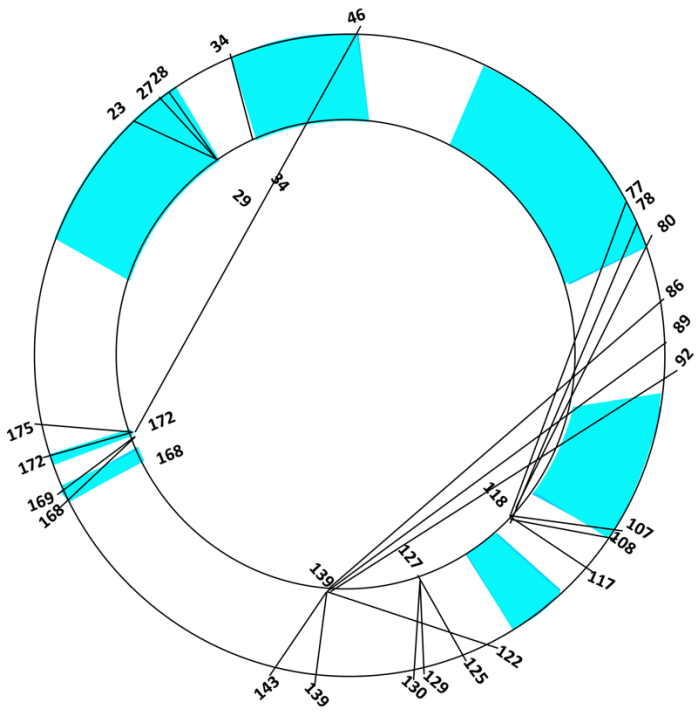

Figure 4 showes the inner circle's candidate functional mutations and the outer circle's interacting residues. According to thecanSAR BLACK system (60), The blue areas represent RhoA functional regions, while the lines linking the inner circle (candidate functional mutation) to the outer circle (interacting residues) represent residue interactions. This figure displays only the HRAS residues that are mutated in cBioPortal.

In cancer samples, four high-scoring RhoA residues (34, 139, 111, and 168) were observed (**see Table 4)**. Residue 34 is near the core area and the GAP interaction site, as per RhoA's 3D structure. A mutation at this location improves the affinity for ARHGAP;1, a GAP protein that plays a vital role in RhoA activation, according to data from ELASPIC (67) and COSMIC. According to COSMIC, mutation 139 of RhoA was observed in one sample of non-small cell lung carcinoma and as a silent mutation in two samples of cervix and stomach cancer— where it was not a functional mutation in the latter two samples. Meanwhile, residue 111 has been seen in one sample of stomach cancer patients (7). Mutation in residue 168 boosts the affinity for the CTRO protein, which regulates cytokinesis by generating a contractile ring. It was also found to interact with KAPCA, a gene associated with breast and ovarian cancer (68). The mutation of residue 168 also

impacted PKN1 and PKN2 interaction with RhoA—two proteins that contribute to prostate cancer and play a crucial role in cell migration and proliferation (69, 70).

DISCUSSION

In this paper, we looked at proteins that are similar and have been classified into families in uniportkb. In terms of sequence, structure, and function, these proteins are very similar. As a result, we assume that the frequent mutations associated with the same cancer phenotype on the same domain share these domains and mutations within the family. As a result, the introduced algorithm employs scores to determine whether these mutations are statistically significant as functional alterations in areas common in families. To test and validate the approach, domains from two well-known protein families (HRAS and RhoA) that are known to be involved in cancer are used.

As a result, we present PhiDsc, a novel method for detecting functional mutations in proteins. To link mutation residues to specific biological functional domains of proteins, we took into account a mutation's position in the protein's 3D structure (71), as well as the frequency of its reoccurrence in human tumors (72). Finally, we combined these characteristics with known functional hotspot mutations aggregated among paralogous proteins in the same family or with similar domains (73), and we used Bonferroni restriction to further narrow the range of predictions in order to reduce false positives..

We evaluated PhiDsc using the HRAS and RhoA proteins (71, 72). HRAS is a GTPase protein in the RAS subfamily that controls many cellular mechanisms including 84 pathways according to KEGG Pathway. The most mutated residues in HRAS are 12, 13, and 61, which are related to different subsets in cancer (73), and the tumorigenic effect of HRAS is related to the protein's

211 permanent activation. RhoA is a RHO subfamily signaling G protein that regulates numerous
212 cellular mechanisms associated with 43 pathways related to cellular processes as seen in KEGG
213 Pathway. The most frequently mutated residues in this protein, 17 and 42, have been observed in
214 various types of cancer (74), and similarly, the oncogenic effect of RhoA is exerted by its constant
215 activation of the protein.

216 With the exception of one candidate residue in RhoA, all residues predicted by PhiDsc were found
217 to be mutated in cancer samples, as well as in other diseases such as Costello syndrome, which is
218 linked to germline HRAS mutations (75). Although certain candidate functional mutations were
219 not previously identified as hotspot mutations and had a low mutated frequency in cancer mutation
220 datasets (rare), using CanSar balck (60), we demonstrated that they were located in active
221 functional domains of proteins or had a wide network of interactions with functional residues.
222 Noteworthy, the Biomuta database was initially used; however, by the final step, some of the
223 candidate functional hotspots that were not found in Biomuta had been presented in tumor samples
224 in other datasets such as COSMIC, cBioPortal, and Dbsnp. With the exception of RhoA residue
225 29, all were identified as rare mutated residues, and, thus, they were not previously mentioned as
226 a hotspots, indicating that PhiDsc improves and optimizes the detection of low frequency
227 functional mutations. while, residue 29 of RhoA had no mutational recorde in COSMIC (46) or
228 Dbsnp (76) databases, mutation analysis software MutaGene (41) ranked RhoA residue 29 as a
229 highly mutable position, and the projected effect by six different software packages at that position
230 predicts a potential oncogenic effect. It is notable that the difference between COSMIC and Dbsnp
231 lies in the curation method used to classify any given mutation as an SNP.

232 Despite the fact that these methods use different concepts to infer the stabilizing effect of point
233 mutations (as discussed in the results section), they all suggest that PhiDsc's predictions alter

protein structure and function. The precise impact of unknown mutations necessitates additional experimental verification.

When DALI was used instead of TM-Align, better results were obtained in PhiDsc with known functional mutations. These findings suggest that different 3D alignment approaches may alter predicting hotspot mutations in different types of proteins. As a result, the PhiDsc package's predictions should improve as the mode of alignment used improves.

Some previously designated hotspots of HRAS and RhoA in cancer, like for HRAS out of 12 (residues 12, 13 and 117) and for RhoA out of 11 (residue 34) were returned by PhiDsc. When the results of the Dali and Tm-Align alignment (supplementary files (HRAS, RHOA) Tm-Align) methods were compared, the results of the Tm-Alignment method predicted fewer well-known driver mutations than the results of the Dali method. This suggests that a different alignment choice could result in some differences in predictions.

Although the two example proteins selected for validation are oncogenic, PhiDsc is not restricted to oncogenes and can be utilized to identify functional mutations in tumor suppressor genes or any other type of Protein if the family has a sufficient number of members and the mutation profile data is adequate and consistent.

The lack of a 3D structure of the protein and small protein families, which limit the number of members in the family, are two limitations of this method. A future update to the tool will include the ability to align functional domains of proteins rather than the entire protein, as well as the use of the protein's predicted 3D structure in the alignment comparison.

MATERIALS AND METHODS

PhiDsc Algorithm

PhiDsc uses a six-step method that is centered on a protein **P** with **m** amino acid residues and a known three-dimensional structure. Briefly, a list of proteins is defined, denoted by the set **A(P)**, by identifying all members of P's protein family from UniProtKB (42) and selecting all human proteins with 3D structures from the Protein Data Bank (PDB) (43). Next, the 3D structures of the proteins members in A(P) are aligned to the 3D structure of P. The results are presented by a matrix, **E(P)**. Then, using the BIOMUTA V4 and 3Dhotspot database (44), the mutational information of each protein of A(P) is identified, in order to score each residue of P and calculate an associated probability. Finally, these are analyzed to identify potential candidate functional mutations in P. Each step is described in detail in what follows.

Step 1: Define the protein list A(P). The UniProtKB database (42) is used to identify members of a given protein's protein family, while the RCSB Protein Data Bank (PDB) (43) is used to determine their three-dimensional structure. The PDB contains the structures of wild-type and mutated proteins. For the alignment step, either the full-length sequence of the wild-type protein or the least mutated form (maximum one mutation) of the same length is used; the final list is denoted by $A(P) = \{P_1, P_2, P_3 \dots P_n\}$.

Step 2: Align 3D structures. Dali, a pairwise comparison server for protein structures, is used to align protein structures (http://ekhidna2.biocenter.helsinki.fi/dali/)(45). TM-Align "another alignment method" is also included in PhiDsc with its default parameters.

Step 3: Define matrix E(P). E(P)= $[a^{j}_{k_{ij}}]$ has n columns (number of proteins) and m rows (number of amino acids in protein P), in which $a^{j}_{k_{ij}}$ denotes the type of amino acid in the sequence of protein

j that is aligned to the i^{th}amino acid in protein P; k_{ij} denotes the position number of amino acid in the sequence Pj that is aligned to the i^{th}amino acid of protein P.

Step 4: Identify mutational information of each protein in A(P). Residues for all protein family members are annotated with mutational and hotspot information using BioMuta (version 4, (10)) and 3Dhotspots (39). BioMuta is a database of curated cancer-associated single-nucleotide variations derived from COSMIC (46), ClinVar (47), CIVIC(48), and UniProtKB(42) and actively curated from publications and automated analysis of publicly available databases such as TCGA(7)and ICGC(8). 3Dhotspots is a dataset of statistically significant mutations clustered in three-dimensional protein structures found in cancer. The data set contains mutational positions referred to as hotspot mutations.

Step 5: Score residues. A grade is assigned to each amino acid of A(P) members based on the mutational information for that amino acid (P). Let a_k^t be the kth amino acids of protein P_t. Define:

$$m(a_k^t) = \begin{cases} 1, & if\ a_k^t\ is\ reported\ as\ mutation\ in\ biomuta \\ 2, & if\ a_k^t\ is\ reported\ as\ hotspot\ in\ 3Dhotspots\ database \\ 0, & otherwise(either\ non-aligned\ or\ not\ mutated) \end{cases}$$

Let the i^{th} row of the matrix E(P) be $[a_{k_{i1}}^1, a_{k_{i2}}^2, \dots, a_{k_{in}}^n]$, $1 \le i \le m$. The following score is assigned to i^{th} amino acids of P:

$$S(i) = \sum_{j=1}^{n} m\left(a_{k_{ij}}^j\right)$$

To calculate the statistical significance of the obtained scores $S(i)$ at each position (row in the matrix E(P)), we calculate the probability related to this score. Let protein P_t have m_t amino acids of which l_t are mutated in biomuta. Define:

$$P(a_k^t) = \begin{cases} \frac{l_t}{m_t} & , m(a_k^t) > 0 \\ 1 - \frac{l_t}{m_t}, & m(a_k^t) = 0 \end{cases}$$

To distinguish non-mutated from the non-aligned residues (both with score $m(a_k^t) = 0$), and because the event under investigation is the occurrence of functional mutations that are coded in the alignments. Then, if in $a_{k_{ij}}^j$ (j) is a gap, we assume $P\left(a_{k_{ij}}^j\right) = 1$.

Then:

$$P\big(S(i)\big) = \Pi_{j=1}^{n} P(a_{k_{ij}}^j)$$

Step 6: Select candidates. The i^{th} amino acid of protein P is selected as a candidate functional mutation if $P\big(S(i)\big)$ is less than $\frac{0.01}{n}$, following the Bonferroni correction, and if $S(i) > \frac{n}{2}$.

The method is schematically described in **Figure 5**

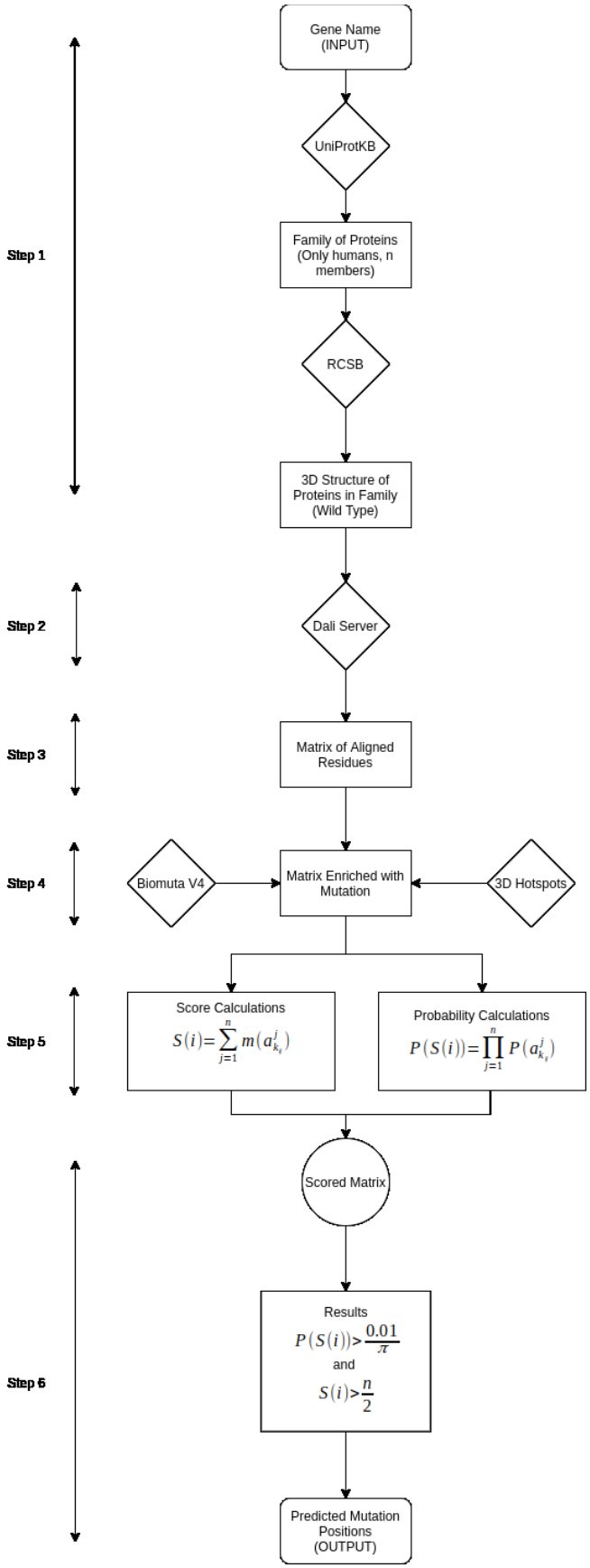

306

Figure 5 The PhiDsc workflow. The system begins by obtaining family members; the algorithm then obtains the 3D structures from RCSB; the algorithm aligns members pairwise with the input protein; mutations are then enriched in the alignments; finally, scores and probabilities are calculated.

Leave-one-out cross-validation

In leave-one-out cross-validation (LOOCV), one data point from the training set remains excluded. For example, if there are n data points in the original sample, n-1 samples are used to train the model, and p points are used as the validation set. This is repeated for all combinations in which the original sample can be separated in this manner, and the error is averaged across all trials to calculate overall effectiveness. The number of possible combinations is equal to the original sample's number of data points, or n.

$A_i(P) = \{P_1, P_2, P_3 \dots P_n\} - \{P_i\}$ is considered as an input set for protein P, and the PhiDsc predictions for P are obtained by considering $A_i(P)$ as its protein family set. The set of predicted functional mutations is obtained for every $1 \leq i \leq n$. A projected functional mutation is said to be robust if it is predicted across at least 80% of all rounds.

Residue Interaction Network

RIN (Residue Interaction Network) is used to quantify the physical effect of the mutation on protein structure and function. In summary, Chang *et al.* demonstrated that if a mutation in a protein's 3D structure is close to some hotspot mutations, the likelihood of this mutation being considered a hotspot mutation is high. The RINalyzer (49) module generates user-defined RINs from a 3D protein structure obtained from RCSB protein databank. RINerator considers different biochemical interaction types, such as contacts/clashes, hydrogen bonds, and hydrogen atoms and quantifies their individual strength as described in Chimera (50). RINalyzer is a Java plugin for Cytoscape(51), a free software platform for the analysis and visualization of molecular interaction

networks. The results of interacting residues from RIN are compared to cBioPortal (11, 12) a dataset of mutations that are curated across cancer samples.

Functional effect of candidate mutations on proteins

The effect of alterations in regions that were not identified as functional mutations experimentally can be calculated using a variety of methods. PhiDsc's functional predictions are evaluated using six methods that, according to Stefl et al. (52), can be classified into three types:

The first group includes machine learning approaches that are trained on protein stability features and account for experimental conditions such as temperature, salt concentration, and pH values. Incorporating such parameters is critical for assessing the free-energy changes caused by mutations under near physiological conditions. This group includes I-Mutant2.0 (53) which uses SVM to estimate ΔΔG upon mutation, and PoPMuSiC-2.0 (54) which uses a mix of statistical potential and neural networks to estimate ΔΔG upon mutation.

The second group relies on evolutionary conservation data, with the assumption that changes at conserved positions in multiple sequence alignments are detrimental. Although these approaches do not directly predict the effect of mutations on protein stability, they are commonly used in conjunction with the methods mentioned above to achieve consensus predictions. This group includes SIFT (55), which uses sequence homology and site conservation to estimate the deleterious effect of mutations, and Provean (56), which predicts the functional impact of all types of protein sequence variations, including single amino acid substitutions, insertions, deletions, and multiple substitutions.

The third group uses structural information, assuming that a protein's ability to function properly is determined by fundamental physicochemical properties that can only be derived from structures.

353 This group includes CUPSAT(57), which estimates ΔΔG upon mutation using mean force atom
354 pair and torsion angle potentials, and MutPred(58), which estimates detrimental effect of mutation
355 using SIFT and gain/loss of structural or functional features predicted from sequences.

356

357 **DATA AVAILABILITY**

358 This method is implemented in Python and the Source code and all tested data can be found on
359 (https://github.com/hobzy987/PhiDSC-DALI). The software takes a UniProt Protein name as
360 input and gives html file as output with aligned residues and probabilities, and a list of all residues
361 sorted according to their score.

362 **ACKNOWLEDGEMENT**

363 The authors thank Dr. Hossein Khiabanian for the insightful discssions and contribution provided
364 for this work.

365

366 **REFERENCES**

367 1. Vogelstein B, Papadopoulos N, Velculescu VE, Zhou S, Diaz LA, Jr., Kinzler KW. Cancer
368 genome landscapes. Science. 2013;339(6127):1546-58.
369 2. Nowell PC. The clonal evolution of tumor cell populations. Science. 1976;194(4260):23-8.
370 3. Hanahan D, Weinberg RA. Hallmarks of cancer: the next generation. cell. 2011;144(5):646-74.
371 4. Martincorena I, Raine KM, Gerstung M, Dawson KJ, Haase K, Van Loo P, et al. Universal
372 patterns of selection in cancer and somatic tissues. Cell. 2017;171(5):1029-41. e21.
373 5. Stratton MR, Campbell PJ, Futreal PA. The cancer genome. Nature. 2009;458(7239):719-24.

374 6. Baeissa H, Benstead-Hume G, Richardson CJ, Pearl FM. Identification and analysis of mutational
375 hotspots in oncogenes and tumour suppressors. Oncotarget. 2017;8(13):21290.
376 7. Tomczak K, Czerwińska P, Wiznerowicz M. The Cancer Genome Atlas (TCGA): an
377 immeasurable source of knowledge. Contemporary oncology. 2015;19(1A):A68.
378 8. Zhang J, Bajari R, Andric D, Gerthoffert F, Lepsa A, Nahal-Bose H, et al. The international
379 cancer genome consortium data portal. Nature biotechnology. 2019;37(4):367-9.
380 9. Consortium APG. AACR Project GENIE: powering precision medicine through an international
381 consortium. Cancer discovery. 2017;7(8):818-31.
382 10. Dingerdissen HM, Torcivia-Rodriguez J, Hu Y, Chang T-C, Mazumder R, Kahsay R. BioMuta
383 and BioXpress: mutation and expression knowledgebases for cancer biomarker discovery. Nucleic acids
384 research. 2018;46(D1):D1128-D36.
385 11. Cerami E, Gao J, Dogrusoz U, Gross BE, Sumer SO, Aksoy BA, et al. The cBio cancer genomics
386 portal: an open platform for exploring multidimensional cancer genomics data. AACR; 2012.
387 12. Gao J, Aksoy BA, Dogrusoz U, Dresdner G, Gross B, Sumer SO, et al. Integrative analysis of
388 complex cancer genomics and clinical profiles using the cBioPortal. Science signaling. 2013;6(269):pl1-
389 pl.
390 13. Martelotto LG, Ng CK, De Filippo MR, Zhang Y, Piscuoglio S, Lim RS, et al. Benchmarking
391 mutation effect prediction algorithms using functionally validated cancer-related missense mutations.
392 2014;15(10):1-20.
393 14. Tchernitchko D, Goossens M, Wajcman HJCc. In silico prediction of the deleterious effect of a
394 mutation: proceed with caution in clinical genetics. 2004;50(11):1974-8.
395 15. Taylor BS, Barretina J, Socci ND, DeCarolis P, Ladanyi M, Meyerson M, et al. Functional copy-
396 number alterations in cancer. PloS one. 2008;3(9):e3179.
397 16. Dietlein F, Weghorn D, Taylor-Weiner A, Richters A, Reardon B, Liu D, et al. Discovery of
398 cancer driver genes based on nucleotide context. bioRxiv. 2018:485292.

17. Alexandrov LB, Nik-Zainal S, Wedge DC, Aparicio SA, Behjati S, Biankin AV, et al. Signatures of mutational processes in human cancer. Nature. 2013;500(7463):415-21.

18. Nik-Zainal S, Davies H, Staaf J, Ramakrishna M, Glodzik D, Zou X, et al. Landscape of somatic mutations in 560 breast cancer whole-genome sequences. Nature. 2016;534(7605):47-54.

19. Chakravorty D, Jana T, Mandal SD, Seth A, Bhattacharya A, Saha S. MYCbase: a database of functional sites and biochemical properties of Myc in both normal and cancer cells. BMC bioinformatics. 2017;18(1):1-10.

20. Chang MT, Bhattarai TS, Schram AM, Bielski CM, Donoghue MT, Jonsson P, et al. Accelerating discovery of functional mutant alleles in cancer. Cancer discovery. 2018;8(2):174-83.

21. Makova KD, Hardison RCJNRG. The effects of chromatin organization on variation in mutation rates in the genome. 2015;16(4):213-23.

22. Lawrence MS, Stojanov P, Polak P, Kryukov GV, Cibulskis K, Sivachenko A, et al. Mutational heterogeneity in cancer and the search for new cancer-associated genes. Nature. 2013;499(7457):214-8.

23. Phan DL, Kim Y, Kim M, editors. MUSIC: Mutation analysis tool with high configurability and extensibility. 2018 IEEE International Conference on Software Testing, Verification and Validation Workshops (ICSTW); 2018: IEEE.

24. Tamborero D, Gonzalez-Perez A, Lopez-Bigas NJB. OncodriveCLUST: exploiting the positional clustering of somatic mutations to identify cancer genes. 2013;29(18):2238-44.

25. Reimand J, Bader GDJMsb. Systematic analysis of somatic mutations in phosphorylation signaling predicts novel cancer drivers. 2013;9(1):637.

26. Miller ML, Reznik E, Gauthier NP, Aksoy BA, Korkut A, Gao J, et al. Pan-cancer analysis of mutation hotspots in protein domains. 2015;1(3):197-209.

27. Cantor AJ, Shah NH, Kuriyan J. Deep mutational analysis reveals functional trade-offs in the sequences of EGFR autophosphorylation sites. Proceedings of the National Academy of Sciences. 2018;115(31):E7303-E12.

424 28. Gao J, Chang MT, Johnsen HC, Gao SP, Sylvester BE, Sumer SO, et al. 3D clusters of somatic
425 mutations in cancer reveal numerous rare mutations as functional targets. 2017;9(1):1-13.
426 29. Chen S, He X, Li R, Duan X, Niu B. HotSpot3D web server: an integrated resource for mutation
427 analysis in protein 3D structures. Bioinformatics. 2020;36(12):3944-6.
428 30. Meyer MJ, Lapcevic R, Romero AE, Yoon M, Das J, Beltrán JF, et al. mutation3D: cancer gene
429 prediction through atomic clustering of coding variants in the structural proteome. Human mutation.
430 2016;37(5):447-56.
431 31. Chen W, Li Y, Wang Z. Evolution of oncogenic signatures of mutation hotspots in tyrosine
432 kinases supports the atavistic hypothesis of cancer. Scientific reports. 2018;8(1):1-8.
433 32. Wang X, Wei X, Thijssen B, Das J, Lipkin SM, Yu H. Three-dimensional reconstruction of
434 protein networks provides insight into human genetic disease. Nature biotechnology. 2012;30(2):159-64.
435 33. Lu H-C, Herrera Braga J, Fraternali FJB. PinSnps: structural and functional analysis of SNPs in
436 the context of protein interaction networks. 2016;32(16):2534-6.
437 34. Gress A, Ramensky V, Büch J, Keller A, Kalinina OV. StructMAn: annotation of single-
438 nucleotide polymorphisms in the structural context. Nucleic acids research. 2016;44(W1):W463-W8.
439 35. Tokheim C, Bhattacharya R, Niknafs N, Gygax DM, Kim R, Ryan M, et al. Exome-Scale
440 Discovery of Hotspot Mutation Regions in Human Cancer Using 3D Protein Structure.
441 2016;76(13):3719-31.
442 36. Ryslik G, Cheng Y, Zhao H. SpacePAC: Identifying mutational clusters in 3D protein space
443 using simulation. 2013.
444 37. Pahari S, Li G, Murthy AK, Liang S, Fragoza R, Yu H, et al. SAAMBE-3D: Predicting effect of
445 mutations on protein–protein interactions. 2020;21(7):2563.
446 38. Wong ET, So V, Guron M, Kuechler ER, Malhis N, Bui JM, et al. Protein–protein interactions
447 mediated by intrinsically disordered protein regions are enriched in missense mutations. Biomolecules.
448 2020;10(8):1097.

449 39. Gao J, Chang MT, Johnsen HC, Gao SP, Sylvester BE, Sumer SO, et al. 3D clusters of somatic
450 mutations in cancer reveal numerous rare mutations as functional targets. Genome medicine. 2017;9(1):1-
451 13.
452 40. Banerjee A, Mitra P. Estimating the Effect of Single-Point Mutations on Protein Thermodynamic
453 Stability and Analyzing the Mutation Landscape of the p53 Protein. Journal of chemical information and
454 modeling. 2020;60(6):3315-23.
455 41. Goncearenco A, Rager SL, Li M, Sang QX, Rogozin IB, Panchenko AR. Exploring background
456 mutational processes to decipher cancer genetic heterogeneity. Nucleic Acids Res. 2017;45(W1):W514-
457 W22.
458 42. Breuza L, Poux S, Estreicher A, Famiglietti ML, Magrane M, Tognolli M, et al. The UniProtKB
459 guide to the human proteome. Database. 2016;2016.
460 43. Burley SK, Bhikadiya C, Bi C, Bittrich S, Chen L, Crichlow GV, et al. RCSB Protein Data Bank:
461 powerful new tools for exploring 3D structures of biological macromolecules for basic and applied
462 research and education in fundamental biology, biomedicine, biotechnology, bioengineering and energy
463 sciences. Nucleic acids research. 2021;49(D1):D437-D51.
464 44. Chang MT, Asthana S, Gao SP, Lee BH, Chapman JS, Kandoth C, et al. Identifying recurrent
465 mutations in cancer reveals widespread lineage diversity and mutational specificity. Nat Biotechnol.
466 2016;34(2):155-63.
467 45. Holm L, Laakso LM. Dali server update. Nucleic acids research. 2016;44(W1):W351-W5.
468 46. Forbes SA, Beare D, Boutselakis H, Bamford S, Bindal N, Tate J, et al. COSMIC: somatic cancer
469 genetics at high-resolution. Nucleic acids research. 2017;45(D1):D777-D83.
470 47. Landrum MJ, Lee JM, Benson M, Brown GR, Chao C, Chitipiralla S, et al. ClinVar: improving
471 access to variant interpretations and supporting evidence. Nucleic acids research. 2018;46(D1):D1062-
472 D7.

48. Griffith M, Spies NC, Krysiak K, McMichael JF, Coffman AC, Danos AM, et al. CIViC is a community knowledgebase for expert crowdsourcing the clinical interpretation of variants in cancer. Nature genetics. 2017;49(2):170-4.

49. Doncheva NT, Klein K, Domingues FS, Albrecht M. Analyzing and visualizing residue networks of protein structures. Trends in biochemical sciences. 2011;36(4):179-82.

50. Pettersen EF, Goddard TD, Huang CC, Couch GS, Greenblatt DM, Meng EC, et al. UCSF Chimera—A visualization system for exploratory research and analysis. 2004;25(13):1605-12.

51. Holmås S, Riudavets Puig R, Acencio ML, Mironov V, Kuiper M. The Cytoscape BioGateway App: explorative network building from an RDF store. Oxford University Press; 2020.

52. Stefl S, Nishi H, Petukh M, Panchenko AR, Alexov E. Molecular mechanisms of disease-causing missense mutations. Journal of molecular biology. 2013;425(21):3919-36.

53. Capriotti E, Fariselli P, Casadio R. I-Mutant2. 0: predicting stability changes upon mutation from the protein sequence or structure. Nucleic acids research. 2005;33(suppl_2):W306-W10.

54. Dehouck Y, Kwasigroch JM, Gilis D, Rooman M. PoPMuSiC 2.1: a web server for the estimation of protein stability changes upon mutation and sequence optimality. BMC bioinformatics. 2011;12(1):1-12.

55. Sim N-L, Kumar P, Hu J, Henikoff S, Schneider G, Ng PC. SIFT web server: predicting effects of amino acid substitutions on proteins. Nucleic acids research. 2012;40(W1):W452-W7.

56. Choi Y, Chan AP. PROVEAN web server: a tool to predict the functional effect of amino acid substitutions and indels. Bioinformatics. 2015;31(16):2745-7.

57. Parthiban V, Gromiha MM, Schomburg D. CUPSAT: prediction of protein stability upon point mutations. Nucleic acids research. 2006;34(suppl_2):W239-W42.

58. Pejaver V, Urresti J, Lugo-Martinez J, Pagel KA, Lin GN, Nam H-J, et al. Inferring the molecular and phenotypic impact of amino acid variants with MutPred2. Nature communications. 2020;11(1):1-13.

59. Kodaz H, Kostek O, Hacioglu MB, Erdogan B, Kodaz CE, Hacibekiroglu I, et al. Frequency of RAS mutations (KRAS, NRAS, HRAS) in human solid cancer. Breast cancer. 2017;7(5).

499 60. Svensmark JH, Brakebusch C. Rho GTPases in cancer: friend or foe? Oncogene.
500 2019;38(50):7447-56.
501 61. Bertola D, Buscarilli M, Stabley DL, Baker L, Doyle D, Bartholomew DW, et al. Phenotypic
502 spectrum of Costello syndrome individuals harboring the rare HRAS mutation p. Gly13Asp. American
503 Journal of Medical Genetics Part A. 2017;173(5):1309-18.
504 62. Gripp KW, Baker L, Robbins KM, Stabley DL, Bellus GA, Kolbe V, et al. The novel duplication
505 HRAS c. 186_206dup p.(Glu62_Arg68dup): clinical and functional aspects. European Journal of Human
506 Genetics. 2020;28(11):1548-54.
507 63. Homami A, Kachoei ZA, Asgarie M, Ghazi F. Analysis of FGFR3 and HRAS genes in patients
508 with bladder cancer. Medical Journal of the Islamic Republic of Iran. 2020;34:108.
509 64. Pozdeyev N, Rose MM, Bowles DW, Schweppe RE, editors. Molecular therapeutics for
510 anaplastic thyroid cancer. Seminars in cancer biology; 2020: Elsevier.
511 65. Gamayunov BN, Korotkiy NG, Baranova EE. Phacomatosis pigmentokeratotica or the
512 Schimmelpenning-Feuerstein-Mims syndrome? Clinical case reports. 2016;4(6):564.
513 66. Kaur HB, Salles DC, Paulk A, Epstein JI, Eshleman JR, Lotan TL. PIN-like ductal carcinoma of
514 the prostate has frequent activating RAS/RAF mutations. Histopathology. 2021;78(2):327-33.
515 67. Witvliet DK, Strokach A, Giraldo-Forero AF, Teyra J, Colak R, Kim PM. ELASPIC web-server:
516 proteome-wide structure-based prediction of mutation effects on protein stability and binding affinity.
517 Bioinformatics. 2016;32(10):1589-91.
518 68. Papanikolaou N, Mantsou A, Kalosidis N. From driver mutations to driver cancer networks: Why
519 we need a new paradigm. Cancer Studies. 2018;2(1):1.
520 69. Scott F, Fala AM, Pennicott LE, Reuillon TD, Massirer KB, Elkins JM, et al. Development of 2-
521 (4-pyridyl)-benzimidazoles as PKN2 chemical tools to probe cancer. Bioorganic & medicinal chemistry
522 letters. 2020;30(8):127040.

523 70. Yang CS, Melhuish TA, Spencer A, Ni L, Hao Y, Jividen K, et al. The protein kinase C super-
524 family member PKN is regulated by mTOR and influences differentiation during prostate cancer
525 progression. The Prostate. 2017;77(15):1452-67.
526 71. Muñoz-Maldonado C, Zimmer Y, Medová M. A comparative analysis of individual RAS
527 mutations in cancer biology. Frontiers in oncology. 2019;9:1088.
528 72. Schaefer A, Reinhard NR, Hordijk PL. Toward understanding RhoGTPase specificity: structure,
529 function and local activation. Small GTPases. 2014;5(2):e968004.
530 73. Mosteller RD, Han J, Broek D. Identification of residues of the H-ras protein critical for
531 functional interaction with guanine nucleotide exchange factors. Molecular and Cellular Biology.
532 1994;14(2):1104-12.
533 74. Kakiuchi M, Nishizawa T, Ueda H, Gotoh K, Tanaka A, Hayashi A, et al. Recurrent gain-of-
534 function mutations of RHOA in diffuse-type gastric carcinoma. Nature genetics. 2014;46(6):583-7.
535 75. Aoki Y, Niihori T, Kawame H, Kurosawa K, Ohashi H, Tanaka Y, et al. Germline mutations in
536 HRAS proto-oncogene cause Costello syndrome. Nature genetics. 2005;37(10):1038-40.
537 76. Sherry ST, Ward M-H, Kholodov M, Baker J, Phan L, Smigielski EM, et al. dbSNP: the NCBI
538 database of genetic variation. Nucleic acids research. 2001;29(1):308-11.

539